Effects of the interface between two Lennard-Jones crystals on the lattice vibrations: a molecular dynamics study

2009 J. Phys.: Condens. Matter 21 345402

(http://iopscience.iop.org/0953-8984/21/34/345402)

J. Phys.: Condens. Matter **21** (2009) 345402 (8pp) doi:10.1088/0953-8984/21/34/345402

Effects of the interface between two Lennard-Jones crystals on the lattice vibrations: a molecular dynamics study

John W Lyver IV[1,2] **and Estela Blaisten-Barojas**[1]

[1] Computational Materials Science Center and Department of Computational and Data Sciences, George Mason University, Fairfax, VA 22030, USA
[2] Office of Safety and Mission Assurance, National Aeronautics and Space Administration, Washington, DC 20546, USA

E-mail: blaisten@gmu.edu

Received 10 June 2009, in final form 19 July 2009
Published 5 August 2009
Online at stacks.iop.org/JPhysCM/21/345402

Abstract
Effects on the density of vibrational states due to the interface created between two types of solid Lennard-Jones systems is investigated as a function of the atomic masses and model potential parameters. The interface is responsible for a depletion of modes at low frequency and an enhancement at higher frequencies when the potential parameters are increased relative to the reference solid. Opposite trends are observed when the atomic mass increases. When a heat current is established across the interface the density of vibrational states at low frequency is increased and the temperature profile across the binary sample displays a discontinuity at the interface, which is more pronounced as the material parameters become more dissimilar. The thermal boundary resistance (Kapitza resistance) increases as the difference between the two material properties increases and decreases with increasing temperature. It is predicted that, as temperature decreases, the Kapitza length increases as T^{-2} at the nanoscale. Plots of the thermal conductivity as a function of temperature for solids with various parameters are provided, all of them showing the expected T^{-1} behavior.

1. Introduction

Large-scale integrated circuitry, components and sensors rely on internal solid–solid interfaces for controlling the operation of the device and on efficient thermal energy management for dissipating heat generated inside the device. It is then important to examine the ability of a device to transport heat when two solids meet at an interface. An appropriate selection of materials could enhance or restrict the flow of thermal energy. Since the discovery of a thermal boundary resistance at cryogenic solid–liquid interfaces by Kapitza [1], researchers have invested efforts in understanding the cause of the thermal resistance and to quantify its magnitude as a function of both material properties and parameters such as temperature and pressure. Solid–solid thermal boundary resistance has often been referred to as the Kapitza resistance (Ω_K). In solids, this boundary resistance plays an important role in determining heat flow, both in cryogenic and room-temperature applications. The acoustic mismatch model (AMM) and the diffuse mismatch model (DMM) [2, 3] are quite accurate for describing thermal transport at a solid–solid interface at low temperatures. It is also accepted that the AMM is more applicable at a few degrees kelvin, while the DMM works better at higher temperatures. However, at intermediate cryogenic temperatures and above, the experimental Ω_K is larger than that predicted by AMM and DMM. These models lack an appropriate description of the phonon scattering caused by various sources located in the immediate proximity of the interface. More recently, several works have used molecular dynamics atomistic simulations to examine properties such as the boundary resistance at flat interfaces Ω_K [4], diffuse scattering of the vibrational states at each side of the interface [3, 5], structural ordering on each side of an interface [3, 4, 6–9] and the effect of mass changes on each side of the interface on the eventual overlapping of vibrational states and energy transport [10, 11].

In parallel to the above-mentioned atomistic work, a number of authors have addressed a variety of non-

equilibrium molecular dynamics (NEMD) techniques and established these methods as the best for the determination of thermal properties in non-homogeneous systems such as grain boundaries [12–16]. For example, NEMD was used for obtaining the lattice thermal conductivity by simulating the directional heat flow perpendicular to infinite thin films in one-, two-or three-dimensional Lennard-Jones (LJ) systems [4–6, 10–19].

NEMD has been used to determine the Kapitza resistance mostly at grain boundaries or one-dimensional systems [4, 5, 16, 18, 20]. Other studies [5, 16, 18, 21, 22] have proposed that the Kapitza effect is due to reflection of the harmonic phonons at the interface or grain boundary, inelastic effects and anharmonicities. References [5, 16] are studies of a silicon grain boundary simulated with the Stillinger–Weber potential. The authors in [18] simulate the interface of two fcc lattices where one solid is composed of LJ atoms and the other of Morse-potential atoms. Reference [21] is a study of the thermal boundary resistance of an LJ system with geometry similar to the one presented in this paper; however, the acoustic mismatch model is used instead of exploiting directly the NEMD computer experiment results. The NEMD was used in [22] to study the temperature jump at a liquid–solid boundary. Based on these few studies, it is apparent that there is no general understanding of the Kapitza resistance as a function of the atomic parameters entering in the modeling of the materials.

This paper addresses the effects of an interface on the atomic vibrations in Lennard-Jones (LJ) solids, without or with a heat current flowing through the solid sample. Selection of the type of materials could limit, encourage or restrict the flow of thermal energy through a solid–solid interface. For example, the effect of compositional disorder on the lattice thermal conductivity (κ) of binary LJ solids was analyzed recently [23]. The present study expands that work by focusing on the thermal boundary resistance occurring at the interface between two LJ solids as a function of the ratio of atomic parameters of these solids (LJ parameters ϵ, σ and mass). This paper is organized as follows: section 2 describes the equilibrium (MD) and non-equilibrium molecular dynamics (NEMD) methodology used and the geometry of the binary LJ system. Section 3 addresses the effects of the solid–solid interfaces on the density of states of lattice vibrations. Results of the lattice thermal conductivity and the thermal boundary resistance as a function of the LJ parameters and mass are presented in section 4. The summary in section 5 concludes this paper.

2. Molecular dynamics approach: equilibrium and non-equilibrium

For all MD simulations a square-prism computational box elongated along the X axis is used with periodic boundary conditions in the two perpendicular directions Y and Z. Atoms within this computational box are initially located in face centered cubic (fcc) lattice sites and the number density is $\rho = 1.07$ at $T = 0.12$ and $\rho = 1.04$ at $T = 0.33$. Next, the computational box is divided in two equal-size elongated prisms. The dividing plane is located at $X = 0$ and each half-box is filled with atoms of either A or B type. An interface develops between these two systems. The interactions between atoms are of LJ type. Atoms on the positive X axis belong to the reference system and have LJ parameters ϵ_A (potential well), σ_A (hard core radius) and atomic mass m_A. Atoms on the negative X axis belong to a system that has either one LJ parameter (ϵ_B, σ_B) or mass (m_B) different from the corresponding parameter of the reference system. Parameters for the LJ interactions between atoms located on each side of the interface follow the combination rules: $\epsilon_{AB} = \sqrt{\epsilon_A \epsilon_B}$ and $\sigma_{AB} = (\sigma_A + \sigma_B)/2$. Typically the computational box contains 2000 atoms of both types located within a prism of size $5 \times 5 \times 20$ fcc unit cells (4 atoms/unit cell).

The orientation of the one-component crystal is set as [100] along the X direction in the computational box. For the two-component system, the [100] orientation is adopted for both components. For B atoms which have a σ parameter different from the A atoms the number of XY planes and XZ planes in the B region is chosen such that the cross section of the computational box containing B atoms is commensurate with the cross section of the prism containing A atoms. Quantities are expressed in reduced units with respect to parameters of the reference A atoms. Thus, units of mass, length, energy, time, temperature, frequency and thermal conductivity are m_A, σ_A, ϵ_A, $t_A = \sqrt{m_A \sigma_A^2/\epsilon_A}$, ϵ_A/k, t_A^{-1} and $k/(\sigma_A t_A)$, respectively (k is the Boltzmann constant). The time step in the molecular dynamic runs is $\Delta t = 0.005$. A radial cutoff of $3.8\sigma_A$ is adopted. When two different LJ systems are in contact, the following values of the parameter ratios are considered: (i) for the parameter ϵ, $R_\epsilon = \epsilon_B/\epsilon_A = 1.0$, 1.25, 1.5 and 2.0; (ii) for the parameter σ, $R_\sigma = \sigma_B/\sigma_A = 1.0$, 1.1 and 1.2 and (iii) for mass, $R_m = m_B/m_A = 1.0$, 1.6, 2.1 and 3.3.

Because the cross-section edges of the computational box are smaller than its length, effects of periodicity could be significant on dynamical properties. To make certain that our results do not contain unrealistic correlations such as correlation relaxation times τ_{relax} exceeding the time τ_{pbc} for spatial translations to become periodic, both of these times were closely monitored. For the monoatomic reference system at $T = 0.12$ and 0.33, calculation of these two times was repeated for various computational box cross sections showing that 5×5 fcc unit cell cross sections (100 atoms) yield a $\tau_{pbc} \approx 2.6 t_A$, which is longer than $\tau_{relax} \approx 0.2 t_A$. The τ_{relax} value is an average over ten different initial times of the velocity autocorrelation function. Thus, effects of the boundary conditions are negligible. All correlation functions used in this work were followed for $512\Delta t$ to avoid uncertainties that begin to increase rapidly for longer times [24, 25]. From the low frequency region of the velocity autocorrelation Fourier transform, an estimate of about 3 is obtained for the sonic velocity.

The non-equilibrium molecular dynamics set-up consists of a simulated thermostat attached at each end of the elongated computational box such that a temperature gradient would develop across the sample. Each thermal bath contains 200 atoms in fcc positions ($5 \times 5 \times 2$ unit cells) continuing

the computational box. Atoms in each thermal bath move according to a constant temperature MD in which their atomic velocities are scaled at every time step to ensure the temperature desired for that bath. Atoms in-between these two thermal bath regions move with iso-energy MD and data are collected only on these central atoms (typically 1400 atoms) located in the prism-shaped computational box. When a temperature drop exists between the two thermal baths, a thermal energy current is established along the prism and the system is neither in thermal equilibrium nor in a steady state. However, after a certain time the system reaches the steady state and the thermal energy current is constant along the length of the computational box in the direction of the energy flow. This NEMD arrangement has been used by other authors in calculations of the lattice thermal conductivity [11–14, 17, 15, 16, 18, 21, 22].

Steady state data of all studied properties are averaged over 100-atom subsets. Atoms in each subset are located in equal-sized regions sliced perpendicular to the computational box length. For the two-component systems (interface at $X = 0$), the type A atoms (reference) are located on the half-portion of the computational box adjacent to the hot thermal bath that contains A-type atoms only. The other half of the prism-shaped box contains atoms of type B, which are adjacent to the colder thermal bath built of B-type atoms only. As a result of the different dynamics between the atoms in the thermostat and the atoms in the active central region where data are taken, a few planes of atoms adjacent to the thermal baths were not considered in the reporting of results. A similar consideration was adopted by other authors [13, 14, 17, 16].

3. Effect of the interface on the lattice vibrations

The velocity autocorrelation function for N atoms is defined as

$$C(t) = \sum_{i=1}^{N} \langle \vec{v}_i(t) \cdot \vec{v}_i(0) \rangle \Big/ \sum_{i=1}^{N} \langle v_i^2(0) \rangle \qquad (1)$$

where v_i are the atom velocities. This $C(t)$ is calculated at different temperatures with iso-energy MD for the monoatomic systems and for the two-component systems containing an interface separating B atoms from the reference A atoms. Typical MD runs are $500\,000\Delta t$ long to reach equilibrium followed by $20\,000\Delta t$ used for building 30 $C(t)$ from sequential time segments. Each $C(t)$ has a length of $512\Delta t$. Two temperatures are investigated: $T = 0.12$ and 0.33. The density of vibrational states (DOS) is obtained from the Fourier transform of $C(t)$ [26]. The normalized DOS of the reference system containing A atoms is shown in figure 1 (solid line). When the LJ parameters are given the values in [27], the DOS in this work compares very well with the published results [26]. Therefore, the elongated shape of the computational box does not affect significantly the distribution of vibrational frequencies.

When the three variable parameters ϵ, σ, m have values different from the A-type atoms, the atomic vibrational frequencies change with respect to the reference system. Figure 1 shows the normalized DOS of systems entirely composed of B atoms with different values of the three variable parameters compared to the DOS of the reference system plotted as a solid line at $T = 0.12$ (figures 1(a)–(c)) and $T = 0.33$ (figures 1(d)–(f)). Figures 1(a) and (d) show the DOS for three values of ϵ_B with the ratio $R_\epsilon = 1.25$ (circles), 1.5 (squares) and 2.0 (triangles) while the other two parameters σ and mass are equal to the reference system ($R_\sigma = R_m = 1$). In the same manner, figures 1(b) and (e) show the DOS of a system in which $R_\sigma = 1.1$ (circles) and 1.2 (squares) and $R_\epsilon = R_m = 1$. Comparison of the reference system DOS with the DOS of a system in which $R_m = 1.6$ (circles), 2.1 (squares) and 3.3 (triangles) and $R_\epsilon = R_\sigma = 1$ is displayed in figures 1(c) and (f). It is evident from these results that there is a strong overlap between the DOS of the reference system (continuous line) and the DOS of systems with different

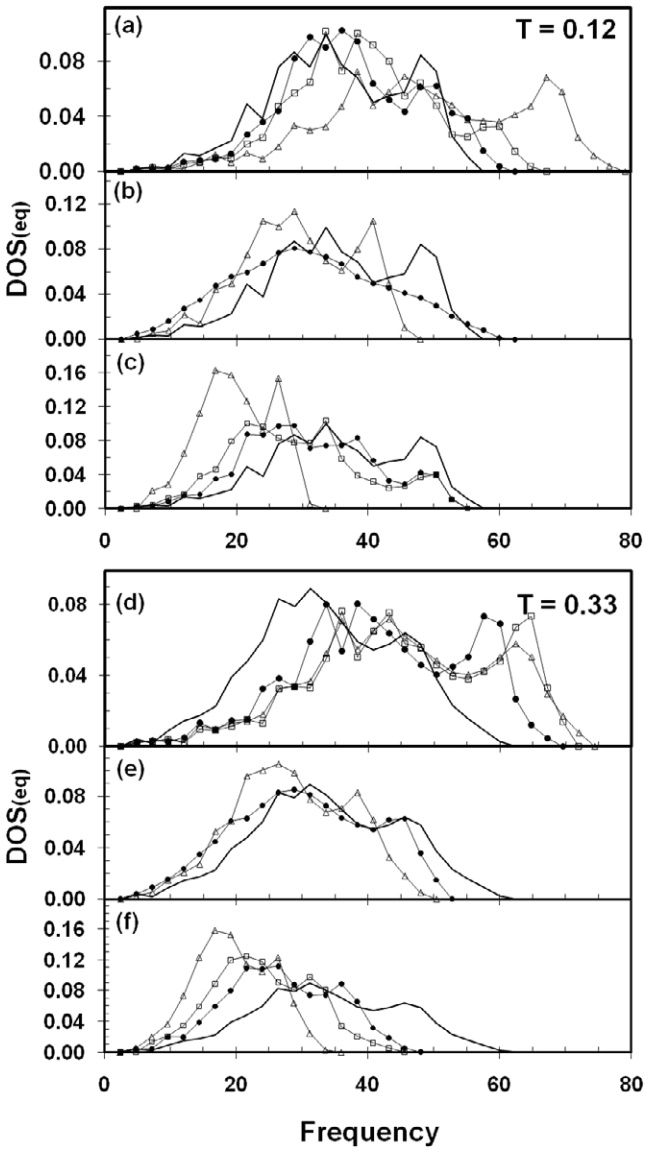

Figure 1. Normalized density of states (DOS) of one-component systems in thermal equilibrium for various LJ parameters. Solid line in all plots pertains to the reference system of A atoms. (a) $R_\epsilon = 1.2$ (●), 1.5 (□), 2.0 (△); (b) $R_\sigma = 1.1$ (●), 1.2 (△); (c) $R_m = 1.6$ (●), 2.1 (□), 3.3 (△).

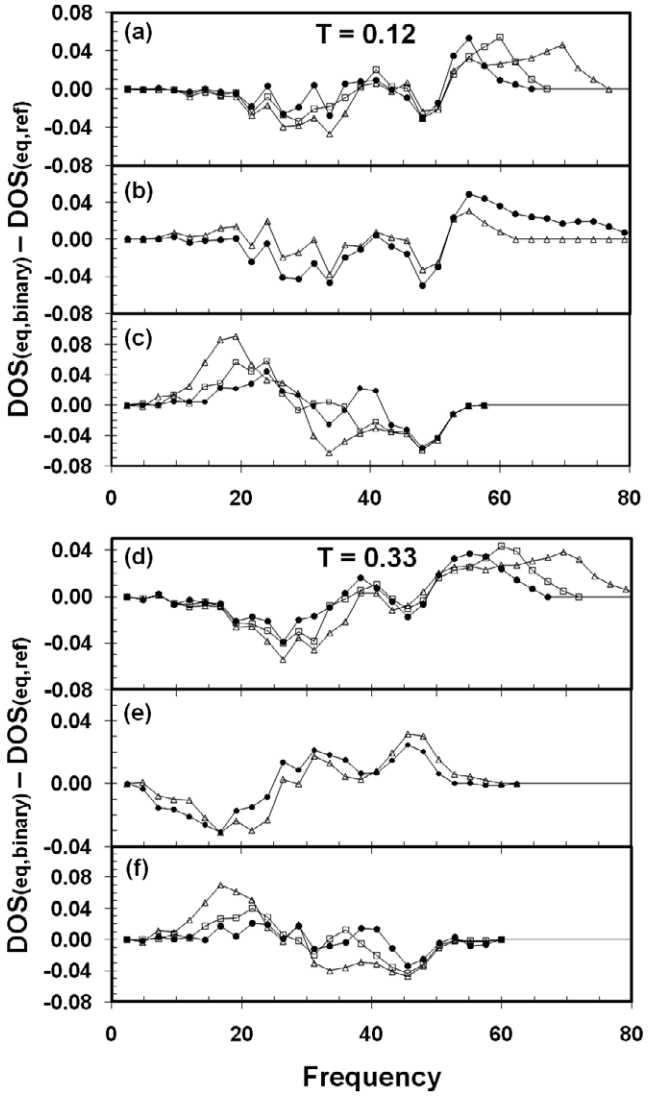

Figure 2. Normalized density of states (DOS) of binary systems in thermal equilibrium relative to the DOS of the one-component reference system for various LJ parameters. (a) $R_\epsilon = 1.2$ (●), 1.5 (□), 2.0 (△); (b) $R_\sigma = 1.1$ (●), 1.2 (△); (c) $R_m = 1.6$ (●), 2.1 (□), 3.3 (△).

parameters. It is to be noted that the DOS is shifted towards smaller frequencies as the mass is increased, which is expected. On the other hand, increases in ϵ and, to a lesser extent, σ with respect to the reference system tend to add high frequency vibrational modes to the DOS.

The presence of an interface affects the DOS. To study this effect, an interface is constructed in the middle of the elongated computational box, perpendicular to its length, by placing A atoms on one-half of the box and B atoms on the other half. Subsequently, this two-component system is equilibrated at two temperatures $T = 0.12$ and 0.33 and the DOS calculated at each of these two temperatures. Figure 2 shows the difference between the normalized DOS of the two-component system calculated for different types of B atoms and the normalized DOS of the reference system containing only A atoms. For interfaces due to changes in ϵ_B, figures 2(a) and (d) show an increase in the DOS of vibration modes at high frequencies

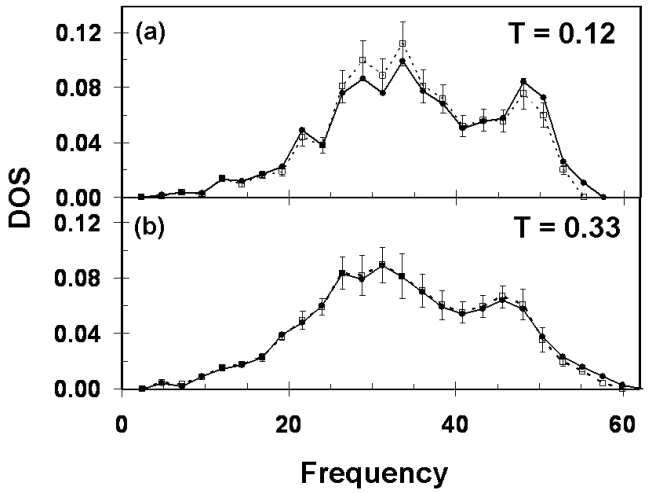

Figure 3. Non-equilibrium DOS of the monoatomic reference system of A atoms (□) compared to the DOS in equilibrium (●) at (a) $T_{avg} = 0.12$; (b) $T_{avg} = 0.33$.

(60–80) and a decrease at lower frequencies around 20–40, both of which persist at $T = 0.33$. The effect is about the same for all R_ϵ values. Interfaces due to the different σ_B shown in figures 2(b) and (e) display DOS changes similar to the changes in ϵ_B but now in different frequency regions. On the other hand, as shown in figures 2(c) and (f), the effect of mass changes produces a depletion of modes in the DOS in the range $30 \leqslant \omega \leqslant 50$ and an increase of mode density in the lower frequency region $10 \leqslant \omega \leqslant 30$. The mass effect is more acute the larger R_m becomes, in agreement with previous findings [11]. In all cases the effect of the interface is identified by DOS changes above and below a characteristic frequency of $\omega_c \approx 30$.

The DOS is also affected when the system is not in thermal equilibrium. To study this effect the reference system composed of only A atoms is connected to the hot and cold thermal baths such that the NEMD set-up allows for the system to reach a steady state after $500\,000\Delta t$. The subsequent $11\,000\Delta t$ are used for production. In the steady state of heat transfer, a temperature gradient develops along the length of the computational box. The temperature at the center of the box is the system average temperature. For this non-equilibrium (NE) system, 16 $C(t)$ of length $512\Delta t$ were sequentially constructed from the production results and the DOS obtained from their Fourier transforms. Figure 3 shows the reference system normalized DOS in thermal equilibrium (filled circles) compared with the non-equilibrium (empty squares) situation at two average temperatures $T = 0.12$ and 0.33. Error bars identify the standard deviation of the sample of 16 correlation functions. It is clearly seen that at the higher temperature the DOS displays marginal changes when the system is in NE. However, at the lower temperature the DOS of the NE system is slightly enhanced around $\omega = 30$. For the binary systems with an interface, figure 4 shows the differences between their NE DOS and the equilibrium DOS. In systems with ϵ and mass changes and at the lower temperature ($T = 0.12$) there is a modest increase of the DOS at frequencies around 30 and a small decrease around 50–60 due to the heat flow. At

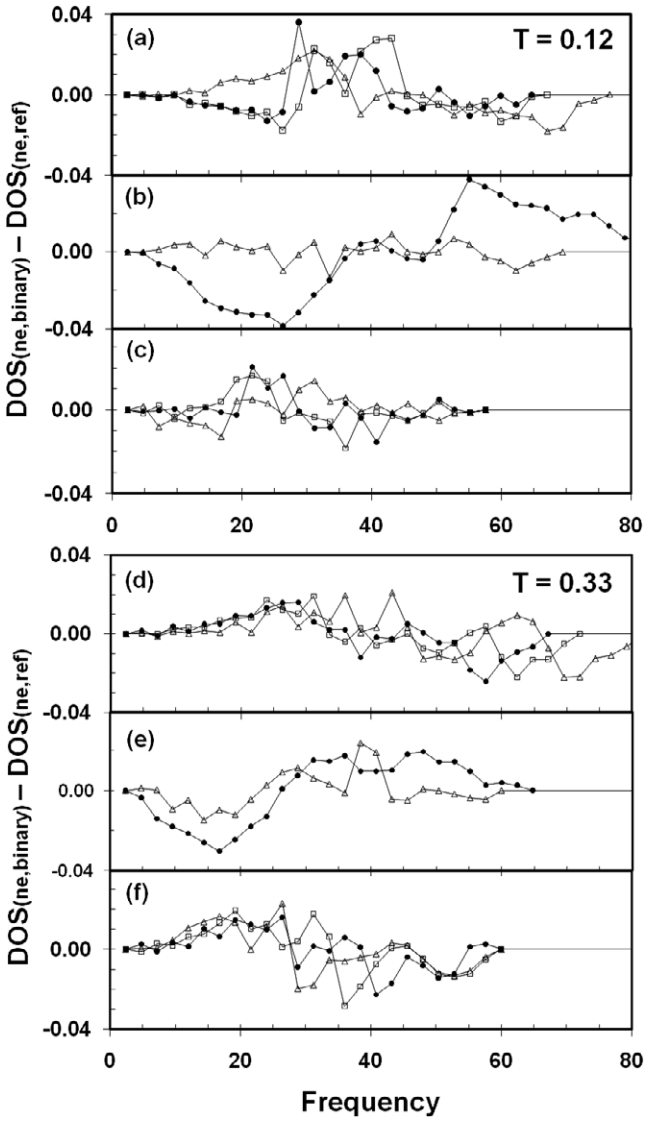

Figure 4. Non-equilibrium DOS of binary systems relative to their DOS in thermal equilibrium for various LJ parameters. (a) $R_\epsilon = 1.2$ (●), 1.5 (□), 2.0 (△); (b) $R_\sigma = 1.1$ (●), 1.2 (×); (c) $R_m = 1.6$ (●), 2.1 (□), 3.3 (△).

$T = 0.33$, the DOS is enhanced in a broader range at the lower frequencies and depleted at higher frequencies for all binary systems involving atoms with two values of the parameter ϵ or the mass. However, two-component systems with different σ (figure 4(b)) display an enhancement of the NE DOS at higher frequencies and a depletion at low frequencies. This effect tends to disappear at higher temperatures.

Summarizing, at $T = 0.12$ the overall effect of a two-atom type interface in equilibrium is to modestly enhance the DOS at frequencies above ω_c and deplete it below this characteristic frequency for R_ϵ, $R_\sigma > 1$ whereas the opposite behavior is demonstrated for $R_m > 1$. When these two-component systems are not in thermal equilibrium, at $T = 0.12$ the trend is an enhancement of the DOS below the ω_c region for systems with different ϵ or mass. This is indicative that the heat flow enhances scattering of the transverse frequency phonons. These trends are smeared out at a higher temperature. On the other hand, interfaces built with atoms that have different σ values display a reverse behavior where the DOS is depleted of modes at frequencies below ω_c and enhanced above it.

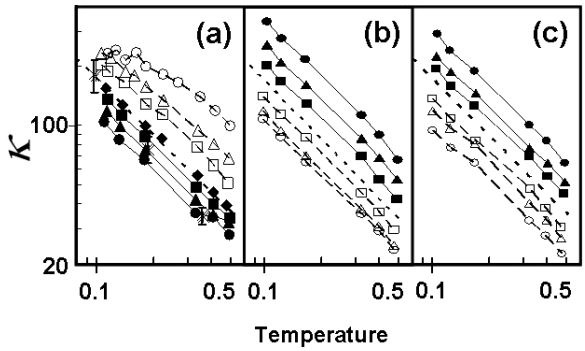

Figure 5. Thermal conductivity as a function of temperature. Solid diamonds pertain to the reference LJ system and dotted line (in (a)–(c)) is the best fit to these values. Crosses and standard deviation are from [23]. (a) $R_\epsilon = 0.7$ (●), 0.8 (▲), 0.9 (■), 1.25 (□), 1.5 (△) and 2.0 (○). Stars and standard deviations are from [23]; (b) $R_\sigma = 0.7$ (●), 0.8 (▲), 0.9 (■), 1.1 (□), 1.2 (△) and 1.25 (○); (c) $R_m = 0.3$ (●), 0.5 (▲), 0.7 (■), 1.6 (□), 2.1 (△) and 3.3 (○).

4. Lattice thermal conductivity and thermal boundary resistance

In the NE situation, a temperature gradient $\vec{\nabla}T$ sets in due to the flow of energy across the computational box. Once the system reaches a steady state, the Fourier law of heat conduction is valid such that

$$\vec{J} = -\kappa \vec{\nabla} T \tag{2}$$

where $\vec{J}$ is the heat current and κ is the lattice thermal conductivity [15, 16]. An atomistic inspection is obtained when $\vec{J}$ is obtained from atomic quantities [28]:

$$\vec{J} = \frac{1}{V}\sum_{i=1}^{N} E_i \vec{v}_i + \frac{1}{2V}\sum_{i=1}^{N}\sum_{j\neq i}^{N} (\vec{v}_i \cdot \vec{F}_{ij})\vec{r}_{ij} \tag{3}$$

where E_i is the total energy of each atom, $\vec{v}_i$ is the velocity of each atom, $\vec{F}_{ij}$ and $\vec{r}_{ij}$ are the forces and interatomic distance vectors between each pair of atoms and V is the volume. Both $\vec{J}$ and $\vec{\nabla}T$ can be calculated in the NEMD set-up described in section 2 and the lattice thermal conductivity κ is then obtained from equation (2). With this geometrical set-up, the heat current components perpendicular to the energy flow should be negligible. Indeed, that is the case in our calculation. The temperature difference between the two thermal baths was chosen to be large with respect to the temperature fluctuations but small enough to reproduce attainable laboratory situations. In our simulations the cold bath temperature is typically about 60% of the hot bath temperature. This choice is similar to the 65%–70% employed in other works [13, 14, 19]. Figure 5 shows the thermal conductivity as a function of temperature for one-component systems with different values of the parameters ϵ, σ and mass. Six different masses and LJ parameters were considered: (i) $R_\epsilon = 0.7$, 0.8, 0.9, 1.25, 1.5 and 2.0

(figure 5(a)); (ii) $R_\sigma = 0.7, 0.8, 0.9, 1.1, 1.2$ and 1.25 (figure 5(b)) and (iii) $R_m = 0.3, 0.5, 0.7, 1.6, 2.1$ and 3.3 (figure 5(c)). In all cases the dotted line corresponds to the reference system $R_\epsilon = R_\sigma = R_m = 1$. Standard deviations are shown on the figure; however, their values of about 3%–7% of the average value are within the size of the symbols. The parameter dependence of κ compares well with our previous work within the Green–Kubo (GK) approach [23]. This alternative method for calculating κ yields large standard deviations at low temperatures, pointing out one of the disadvantages of the GK versus the NEMD approach. The expected inverse temperature relationship for crystalline systems is clearly shown by the log–log plot of figure 5. This can be exploited to interpolate between different LJ systems, as also suggested by other authors [4, 5, 16, 18, 21, 22]. Based on our results such an interpolation yields a power law relationship for each varied parameter (ϵ, σ, mass): $R_\epsilon^{3/2}$, R_σ^{-2} and $R_m^{-1/2}$.

It is well known that solid–solid and liquid–solid interfaces act as a resistance to the heat flow perpendicular to them and give rise to the Kapitza resistance (Ω_K). This effect is measurable because of the discontinuity in the temperature profile occurring at the interface. Such temperature discontinuity is quite distinct across an interface built with two types of atoms and is detectable even for 1D systems where atoms are linked harmonically [4]. Our calculation focuses on Ω_K of binary LJ solid–solid interfaces as a function of ϵ, σ and atomic mass. Figure 6 shows a typical temperature profile at $T = 0.3 (R_m = 3.3, R_\epsilon = R_\sigma = 1)$ where the temperature discontinuity at the interface $\Delta T_{\text{interface}}$ is clearly seen. Following [16], Ω_K is calculated as

$$\frac{1}{\Omega_K} = \kappa_0 \frac{\nabla T}{\Delta T_{\text{interface}}} \tag{4}$$

where κ_0 is the bulk thermal conductivity. However, since we know the κ on each side of the solid–solid interface, the atomistic approach for calculating Ω_K is to use the actual κ and ∇T values for the LJ crystal on each side of the interface. In fact, a thermal current sees the interface as two resistances in series because the heat current must be the same on both sides of the interface if no additional energy sources or sinks exist. It follows that

$$\Omega_K = \Delta T_{\text{interface}} \left(\frac{1}{\kappa_A \nabla T_A} + \frac{1}{\kappa_B \nabla T_B} \right) \tag{5}$$

where $\kappa_{A,B}$ and $\nabla T_{A,B}$ are the thermal conductivity and temperature gradient of the LJ systems A and B that meet at the interface. Figure 7 shows the dependence of the temperature jump $\Delta T_{\text{interface}}$ at the interface and the resulting Ω_K of the two-component systems for various temperatures and parameter ratios. It is observed that, as the parameter ratio moves away from the 1:1 ratio (no interface), the temperature discontinuity and the Ω_K become more pronounced. Additionally, as the average temperature in the system is increased, the interface temperature discontinuity and the Kapitza resistance are less pronounced. It can also be seen that the Ω_K increases at about the same rate with changes of R_ϵ, R_σ, or R_m. In general,

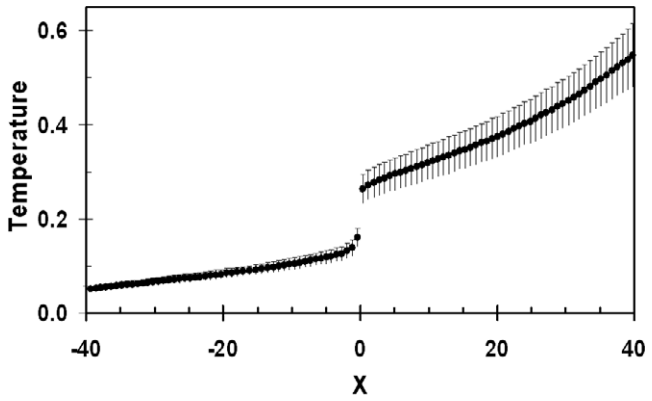

Figure 6. Temperature profile of the NE LJ system with interface at $X = 0$ and $R_m = 3.3$ at average temperature $T = 0.33$. Error bars are the standard deviation of the NEMD run.

the building up of this thermal resistance is assigned to an increased reflectance of phonons by the interface [3, 21]. As discussed in section 3 and shown in figure 2, our equilibrium MD simulation shows that the interface increases the DOS of vibrational states in the region of high frequencies for two-component systems with different ϵ or σ but for systems with different masses the increase occurs at lower frequencies. Based on these results, it immediately follows that two-component systems with different ϵ or σ should display larger Ω_K than the case with different masses at the same temperature. Illustrated in figure 7 is a confirmation of this result. However, in the non-equilibrium situation, when the system reaches the steady state, the DOS of vibrational states is significantly populated in the region of ω_c only for systems with different ϵ and mass, as shown in figure 4. Based on this result, it is then expected that the $\Delta T_{\text{interface}}$ for two-component systems with different ϵ and mass would be larger than for systems with different σ, as is shown in figure 7. Increasing the temperature should reduce the Kapitza resistance and the temperature jump at the interface should be decreased. Our results confirm both effects.

An additional characteristic quantity of interfaces is the Kapitza length $l_K = \kappa \Omega_K$ associated with the effective thickness of material involved in the interface [1, 22]. It has been theorized [22] that, when κ is large, l_K will be large and the effect may be observed but no data were provided for supporting this ansatz. In the example of figure 6, values of κ and Ω_K are 32 and 0.3, respectively, yielding an l_K of about 9. This example was studied for several lengths of the computational prism to determine their eventual effect on l_K. The Ω_K calculated for prism-shaped computational boxes with lengths of 42.3, 73.7, 105 and 136.4 were all within the standard deviation of 11.4%, indicating that this property is basically insensitive to the length of the computational prism and the temperature jump at the interface is observed in all cases. From our results summarized in figures 5 and 7, we predict that l_K varies as $1/T^2$.

We also studied the effect on κ and Ω_K due to changes in the orientation of the crystals on each side of the interface. First, it was determined that one-component systems did not

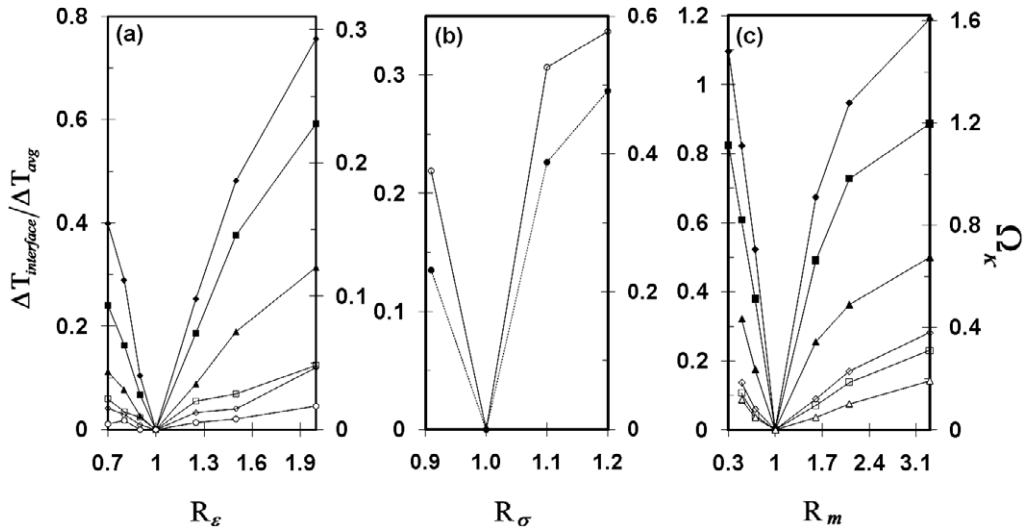

Figure 7. Temperature drop at the interface and Kapitza resistance as a function of system parameters at various temperatures 0.10 (♦), 0.125 (■), 0.165 (▲), 0.33 (□), 0.425 (◊) and 0.5 (○). Temperate drops are plotted relative to the temperature difference between the hot and cold thermal baths.

give rise to a discontinuity in the temperature at the interface when the interface was created by rotating atoms in half of the box to Miller indices [110], [111], [120], [121] and [122] while keeping atoms in the other half of the box at [100] (reference system). Second, the κ for these rotated systems is within the standard deviation of values reported in figure 5. Third, in the case of two-component systems in which the A system is in the [100] orientation and the B system is rotated and its parameters change, the results for the temperature jump and the Ω_K are within 3%–9% of values reported in figure 7. Based on these calculations, we conclude that the relative orientation of the crystal planes meeting at the interface do not affect the thermal properties.

5. Conclusions

In this work we have quantitatively demonstrated the influence of a two-atom type interface between two LJ solid systems on the density of vibrational states as a function of the atomic mass and LJ parameters. A characteristic frequency of $\omega_c = 30$ is predicted below which the DOS is depleted and enhanced above it for R_ϵ, $R_\sigma > 1$ while the opposite behavior is demonstrated for $R_m > 1$. However, when a thermal energy flow is established the DOS is enhanced below ω_c and depleted above it for the cases R_ϵ, $R_m > 1$. This is indicative that the heat flow enhances scattering of the transverse frequency phonons only in these two cases. At higher temperatures these effects are less visible.

The NEMD computer experiment of two-component LJ systems sharing an interface leads to very clear observations that allow for identification of the thermal boundary resistance and its dependence on the LJ parameters and atomic mass. Both the Kapitza resistance and the temperature discontinuity at the interface increase as the parameter ratio between properties of the targeted material to the reference material moves away from the value of one. Additionally, both the Kapitza resistance and the interface temperature discontinuity increase with decreasing temperature. We predict that the Kapitza length increases as $1/T^2$ as the temperature is decreased and is independent of the size of the computational box. The relationships contained in this paper may serve as a reference for scientists and engineers in search of novel combinations of materials in problems related to thermal management at the nanoscale.

Acknowledgments

This work was supported in part by the National Science Foundation, grant CHE-0626111. We acknowledge the Supercomputing Center of the College of Science of George Mason University for the computer time and facilities allocated to this project.

References

[1] Kapitza P L 1941 *J. Phys.* **4** 181
[2] Khalatnikov I M 1952 *J. Exp. Theor. Phys.* **22** 687
[3] Swartz E T and Pohl R O 1989 *Rev. Mod. Phys.* **61** 605
[4] Lumpkin M E, Saslow W M and Visscher W M 1978 *Phys. Rev.* B **17** 4295
[5] Schelling P K, Phillpot S P and Keblinski P 2004 *J. Appl. Phys.* **95** 6082
[6] Liang X-G and Shi B 2000 *Mater. Sci. Eng.* A **292** 198
[7] Young D A, Thomsen C, Grahn H T, Maris H J and Tauc J 1986 *Phonon Scattering in Condensed Matter* (Berlin: Springer) p 49
[8] Stoner R J and Maris H J 1993 *Phys. Rev.* B **48** 16373
[9] Chen G, Tien C L, Wu X and Smith J S 1994 *J. Heat Transfer* **116** 325
[10] Matsumoto M, Wakabayashi H and Makino T 2005 *Heat Transfer Asian Res.* **34** 135
[11] Liang X-G and Sun L 2005 *Micros. Thermophys. Eng.* **9** 295
[12] Nishiguchi N and Sakuma T 1990 *J. Phys.: Condens. Matter* **2** 7575

[13] Lukes J R, Li D Y, Liang X G and Tien C L 2000 *Trans. ASME* C **122** 536
[14] Imamura K, Tanaka Y, Nishiguchi N and Maris H J 2003 *J. Phys.: Condens. Matter* **15** 8679
[15] Phillpot S R, Schelling P K and Keblinski P 2005 *J. Mater. Sci.* **40** 3143
[16] Maiti A, Mahan G D and Pantelides S T 1997 *Solid State Commun.* **102** 517
[17] Mountain R D and MacDonald R A 1983 *Phys. Rev.* B **28** 3022
[18] Twu C-J and Ho J-R 2002 *Phys. Rev.* B **67** 205422
[19] Chantrenne P and Barrat J L 2004 *J. Heat Transfer* **126** 577
[20] Amrit J 2006 *J. Phys. D: Appl. Phys.* **39** 4472
[21] Stevens R J, Zhigilei L V and Norris P M 2007 *Int. J. Heat Mass Transfer* **50** 3977
[22] Barrat J L and Chiaruttini F 2003 *Mol. Phys.* **101** 1605
[23] Lyver J W and Blaisten-Barojas E 2006 *Acta Mater.* **54** 4633
[24] Alder B J and van Thiel M 1963 *Phys. Lett.* **7** 317
[25] Zwanzig R and Ailawadi N K 1969 *Phys. Rev.* **182** 280
[26] Dickey J M and Paskin A 1969 *Phys. Rev.* **188–3** 1407
[27] Grindley J and Howard R 1965 *Lattice Dynamics* ed R F Wallis (New York: Pergamon) p 129
[28] Balescu R 1990 *Equilibrium and Non-Equilibrium Statistical Mechanics* (New York: Wiley) chapter 12